Nonlinear increases in extreme temperatures paradoxically dampen increases in extreme humid-heat

Environmental Research Letters

LETTER

Nonlinear increases in extreme temperatures paradoxically dampen increases in extreme humid-heat

Ethan D Coffel[1,2,3], **Radley M Horton**[4], **Jonathan M Winter**[2,3] and **Justin S Mankin**[2,3,4]

[1] Neukom Institute, Dartmouth College, United States of America
[2] Department of Geography, Dartmouth College, United States of America
[3] Department of Earth Sciences, Dartmouth College, United States of America
[4] Lamont-Doherty Earth Observatory of Columbia University, United States of America

E-mail: ecoffel@dartmouth.edu

Keywords: climate change, extreme heat, humidity, land-atmosphere coupling

Supplementary material for this article is available online

OPEN ACCESS

RECEIVED
12 February 2019

REVISED
8 June 2019

ACCEPTED FOR PUBLICATION
11 June 2019

PUBLISHED
22 July 2019

Abstract

Nonlinear increases in warm season temperatures are projected for many regions, a phenomenon we show to be associated with relative surface drying. However, negative human health impacts are physiologically linked to combinations of high temperatures and high humidity. Since the amplified warming and drying are concurrent, the net effect on humid-heat, as measured by the wet bulb temperature (T_W), is uncertain. We demonstrate that globally, on the hottest days of the year, the positive effect of amplified warming on T_W is counterbalanced by a larger negative effect resulting from drying. As a result, the largest increases in T_W and T_x do not occur on the same days. Compared to a world with linear temperature change, the drying associated with nonlinear warming dampens mid-latitude T_W increases by up to 0.5 °C, and also dampens the rise in frequency of dangerous humid-heat ($T_W > 27$ °C) by up to 5 d per year in parts of North America and Europe. Our results highlight the opposing interactions among temperature and humidity changes and their effects on T_W, and point to the importance of constraining uncertainty in hydrological and warm season humidity changes to best position the management of future humid-heat risks.

Introduction

Humid-heat extremes pose a severe risk to human health [1, 2], and temperature extremes more broadly can reduce economic performance [3, 4], damage crops and ecosystems [5–7], and harm infrastructure [8–10]. Climate change is increasing global mean temperature by altering the surface radiative balance, raising the chances of extreme heat events across the world [11–14]. At regional scales, land-atmosphere interactions among soil moisture and vegetation control the partitioning of energy into sensible and latent heat fluxes, playing a significant role in controlling extreme temperatures, drought, and heat wave statistics in the observational record and in climate models [15–22]. Further, recent research has identified soil drying and associated changes in surface energy partitioning to be a crucial driver of nonlinear temperature changes relative to the warm season mean [23]. In some regions, climate models project that extreme temperatures will increase an additional 1 °C–2 °C beyond warm season mean temperatures—indicating that mean changes alone cannot account for changes in the tails. This amplified warming of temperature extremes has been linked to declines in the fraction of total surface energy fluxes from latent heat, so that in regions where the surface is projected to dry, temperatures are projected to warm more rapidly as more energy is partitioned to sensible heating of the air [23].

While high temperatures have diverse and serious impacts on economies and ecosystems, human health is most tightly linked to the physiological consequences of extreme humid-heat [1]. Constraining uncertainty in the response of humid-heat to climate warming is an urgent task, as recent research has suggested that a critical threshold for human humid-heat tolerance could be approached or exceeded in parts of the world during the 21st century [24–28]. This

Table 1. Selected CMIP5 models.

Model	Organization	Native Resolution
ACCESS1-0	Commonwealth Scientific and Industrial Research Organisation	1.25° × 1.875°
ACCESS1-3	Commonwealth Scientific and Industrial Research Organisation	1.25° × 1.875°
BCC-CSM1-1-M	Beijing Climate Center	2.7906° × 2.8125°
BNU-ESM	College of Global Change and Earth System Science, Beijing, Normal University	2.7906° × 2.8125°
CANESM-2	Canadian Centre for Climate Modelling and Analysis	2.7906° × 2.8125°
CSIRO-MK3-6-0	Commonwealth Scientific and Industrial Research Organisation	1.8653° × 1.875°
CNRM-CM5	Centre National de Recherches Meteorologiques/Centre Europeen de Recherche et Formation Avancee en Calcul Scientifique	1.4008° × 1.40625°
FGOALS-G2	State Key Laboratory for Numerical Modeling for Atmospheric Science and Geophysical Fluid Dynamics	2.7906° × 2.8125°
GFDL-ESM2G	NOAA Geophysical Fluid Dynamics Laboratory	2.0225° × 2.0°
GFDL-ESM2M	NOAA Geophysical Fluid Dynamics Laboratory	2.0225° × 2.5°
HADGEM2-CC	Met Office Hadley Center	1.25° × 1.875°
HADGEM2-ES	Met Office Hadley Center	1.25° × 1.875°
IPSL-CM5A-MR	Institut Pierre Simon Laplace	1.25° × 2.5°
MIROC5	International Centre for Earth Simulation	1.4008° × 1.40625°
MRI-CGCM3	Meteorological Research Institute	1.12148° × 1.125°
NORESM1-M	Norwegian Climate Centre	1.8947° × 2.5°

threshold is defined using the wet bulb temperature (T_W), the saturation temperature of an air parcel. When T_W exceeds the human skin temperature, approximately 35 °C, evaporative cooling is no longer effective as a means of shedding body heat. Prolonged exposure to such conditions causes heat illness and eventually death [29]. In addition, much lower T_W values between 27 °C and 32 °C have routinely caused tens of thousands of deaths and serious heat-related illnesses in recent decades [2], particularly among the world's most vulnerable populations. Uncertainty of a few degrees Celsius at the warm tail of the T_W distribution is therefore essential to constrain, as the mortality risks it poses to people are considerable.

Recent research has shown that anomalously high specific humidity, rather than temperature, is often the dominant driver of present-day extreme humid-heat events [30], while a dry land surface often accompanies the extreme temperature events projected in climate models [31, 32]. Because T_W is nonlinearly dependent on both temperature and humidity, it is not evident how the competing effects of temperature (and its associated surface drying) will combine with specific humidity to alter future risks of extreme humid-heat. Simultaneous changes in these quantities complicate estimates of the T_W response, as temperature and specific humidity not only influence T_W individually, but are also themselves interactive, responding in opposite directions to surface drying (temperature increases more, specific humidity increases less). These direct and indirect effects of temperature and humidity on T_W suggest that surface drying could either increase or decrease humid-heat, depending on the balance of the two changes.

We use daily maximum temperature (T_x) amplification, the nonlinear change in temperature that results in the top half of the T_x distribution warming more than the warm season average (or median) T_x, which appear to be driven largely by land-atmosphere interactions, to assess whether they lead to nonlinear T_W changes in a suite of global climate models. We investigate the relationships between T_x amplification and its associated specific humidity change in the context of land-surface drying, and demonstrate the dependence of the magnitude and frequency of extreme T_W on each at global and regional scales. We then illustrate how T_x amplification-driven changes in T_W affect the frequency of and population exposure to humid-heat extremes.

Data and methods

We utilize climate projections from a suite of 16 global climate models (GCMs) from the Coupled Model Intercomparison Project Phase 5 (CMIP5) [33]. All models that provide the requisite variables for computing daily T_W (daily maximum temperature (Tasmax), specific humidity (Huss), and sea level pressure (Psl)), as well as daily sensible (Hfss) and latent heat fluxes (Hfls), are used (supplementary material table 1). Sea level pressure is used as opposed to true surface pressure due to its greater availability in the CMIP5 ensemble; the difference in pressure is found to have a less than 0.2 °C effect on global T_W estimates, and a still smaller effect for T_W extremes which occur almost exclusively in regions near sea-level. All model projections are made in the period 2061–2085 and are compared with historical simulations spanning 1981–2005. The Representative Concentration Pathway (RCP) 8.5 [34] emissions scenario is used to maximize the climate change signal. All model data are regridded using a linear interpolation procedure to a 2° × 2° resolution to facilitate inter-model spatial comparison. This resolution is generally in the middle of the native CMIP5 model resolutions (see table 1)

and ensures that the models are not all being unphysically downscaled. All analysis is conducted on the locally-defined warm season, estimated for each model and each grid cell as all unique months in which the annual maximum air temperature (TX_x) has occurred during the historical period. The regridding procedure has minimal effect on the model-estimated timing of the warm season (see supplementary material figure S1, which is available online at stacks.iop.org/ERL/14/084003/mmedia).

Daily T_W at the time of maximum air temperature is calculated between 60 °S and 60 °N using the algorithm presented in Davies-Jones, 2008 [35], implemented in HumanIndexMod [36], and ported to Matlab [37]. Estimating T_W at the time of maximum air temperature rather than the true daily maximum T_W creates a negligible downward bias in T_W [24].

Changes in T_x and T_W decile thresholds are calculated for each grid cell and for each model. The resulting changes are averaged over all land grid cells between 60 °S and 60 °N. T_x amplification is calculated for different percentiles. For example, T_x amplification on the TX_x (annual maximum daily temperature) day is calculated for each model and each grid cell as the projected change in TX_x (averaged across all years) minus the projected change in the warm season 50th percentile T_x (also averaged across all years). We denote this amplification using the following notation:

$$\Delta TX_x - \Delta T_x 50,$$

where ΔTX_x is the average change in TX_x (i.e. 100th percentile of the annual T_x distribution) and $\Delta T_x 50$ is the average change in the 50th percentile of the T_x distribution. T_W amplification on the T_{Ww} day is calculated similarly as the change in the annual maximum T_W minus the change in the warm season 50th percentile daily maximum T_W. We similarly denote this amplification as:

$$\Delta T_{Ww} - \Delta T_W 50.$$

We note that our results are robust to the choice of defining amplification ($\Delta TX_x - \Delta T_x 50$ or $\Delta T_{Ww} - \Delta T_W 50$) as relative to the warm season 50th percentile or to the warm season mean.

T_x amplification on the T_{Ww} day is calculated as the projected change in T_x on the day of the annual maximum T_W minus the projected change in warm season 50th percentile T_x. We denote this amplification as:

$$\Delta(T_x|T_{Ww}) - \Delta T_x 50.$$

Similarly, T_W amplification on the TX_x day is calculated as the projected change in T_W on the TX_x day minus the projected change in the warm season 50th percentile T_W, denoted as:

$$\Delta(T_W|TX_x) - \Delta T_W 50$$

T_x amplification across the T_W distribution is calculated as the mean projected change in T_x on all days in each warm season T_W decile ($T_W D$, where D is the decile in which the calculation is being performed) minus the warm season 50th percentile change in T_x:

$$\Delta(T_x|T_W D) - \Delta T_x 50.$$

Similarly, T_W amplification across the T_x distribution is calculated as the mean projected change in T_W on all days in each warm season T_x decile minus the warm season 50th percentile change in T_W:

$$\Delta(T_W|T_x D) - \Delta T_W 50.$$

We also assess specific humidity (Huss) and evaporative fraction (EF) amplification across the T_x and T_W distributions. The EF is the ratio of the latent heat flux to the total heat flux, defined as:

$$EF = \frac{Q_E}{Q_E + Q_H},$$

where Q_E is the latent heat flux, and Q_H is the sensible heat flux. As above, we denote these specific humidity and EF amplifications as:

The specific humidity amplification across the T_x distribution:

$$\Delta(Huss|T_x D) - \Delta(Huss|T_x 50).$$

The specific humidity amplification across the T_W distribution:

$$\Delta(Huss|T_W D) - \Delta(Huss|T_W 50).$$

The EF amplification across the T_x distribution:

$$\Delta(EF|T_x D) - \Delta(EF|T_x 50).$$

The EF amplification across the T_W distribution

$$\Delta(EF|T_W D) - \Delta(EF|T_W 50).$$

To estimate the effect of T_x amplification's temperature component on T_W, for each model and for each grid cell, we calculate the T_W change on days in each decile of the T_x distribution using the decile's projected T_x change and the specific humidity change at the T_x median. To estimate the effect of T_x amplification's specific humidity component on T_W, we repeat the calculation using each T_x decile's projected specific humidity change and median T_x change. The total effect of T_x amplification on T_W change is estimated by repeating the calculation for each T_x decile's projected specific humidity change and each decile's projected T_x change. The components of T_W change due to temperature and specific humidity change are calculated by subtracting the median T_W change from the mean of the T_W change across the top five T_x deciles.

The number of days per warm season that exceed T_W thresholds is estimated using our calculations of T_x amplification-driven changes in T_W. Model bias in absolute T_W is removed via a percentile-matching procedure using the ERA-Interim reanalysis. For each selected T_W threshold, the corresponding T_W percentile is found for each grid cell in ERA-Interim T_W data. The number of days per warm season that exceed this T_W percentile is then calculated for each model and

each grid cell in historical climate simulations. Next, future T_W values including the effects of T_x amplification are calculated for each model, grid cell, and decile by adding the decile-mean change to the model's historical decile-mean T_W value, and the number of days exceeding the same T_W percentile is calculated using this future T_W distribution. Future T_W values not including the effects of T_x amplification are calculated for each model, grid cell, and decile by adding the 50th-decile-mean T_W change to the model's historical decile-mean T_W values in each decile, and the number of days exceeding the same T_W percentile is calculated. Finally, the number of additional days exceeding the T_W threshold due to T_x amplification is calculated by subtracting the number of exceedances calculated without the effects of T_x amplification from the number of exceedances calculated with the effects of T_x amplification.

Population exposure to each T_W threshold is estimated using spatially explicit population projections from the Shared Socioeconomic Pathways Project [38, 39]. Results are shown using the SSP3 population trajectory, which is consistent with the RCP 8.5 emissions scenario. For each model and each grid cell, the population change averaged over 2060–2090 as compared to 2010 is multiplied by the change in the number of extreme T_W exceedances at each T_W threshold between 27 °C and 31 °C, giving humid-heat exposure in the units of person-days per year. These exposure totals are summed for all global grid cells.

Results and discussion

We define an amplification to be the projected change in T_x, T_W, or other climate variables at a particular point in the distribution relative to the projected change in that variable at the 50th percentile across the local warm season. Positive (negative) amplification is when the magnitude of the local warm season change in percentiles above the 50th percentile is greater (less) than the magnitude of change at the 50th percentile. Positive (negative) amplification implies that there is not simply a mean shift in the distribution, but also an increase (decrease) in the variance of the right tail.

Global-scale nonlinear increases in warm temperatures are apparent by 2061–2085 across the 16 CMIP5 models forced with RCP 8.5 (see Methods). T_x changes are negatively amplified for percentiles below the local warm season's 50th T_x percentile and positively amplified for percentiles above it (figure 1(a)). In contrast, warm season T_W changes show less variation across the T_W distribution, suggesting a mean shift in response to forcing. The multi-model median globally-averaged T_x amplification on the TX_x day (the 100th T_x percentile in each year; $\Delta TX_x - \Delta T_x50$) is 0.34 °C, bringing the total TX_x change to over 4.5 °C, but shows wide spatial variation, with parts of the eastern and southwestern US, northern Europe, and China exhibiting well over a degree of amplification (figure 1(b)). This positively-amplified warming of high T_x values at both global and regional scales has been linked to land-atmosphere coupling and land surface drying [23], which allows energy to be preferentially partitioned into sensible rather than latent heat flux. T_W, despite having temperature as a contributing factor (along with humidity and atmospheric pressure), exhibits less amplification than T_x across the globally-averaged distribution: the multi-model median annual maximum T_{Ww} day (the 100th T_w percentile in each year; $\Delta T_{Ww} - \Delta T_W50$) rises 0.24 °C more than the warm season 50th percentile T_W (figure 1(c)). Parts of North Africa and the Middle East have amplified T_W of just under a degree Celsius, though the magnitudes and ubiquity of T_W amplification (figure 1(c)) is less than that for T_x amplification (figure 1(b)).

As global temperatures rise, the multi-model median projects that T_x on the T_{Ww} day ($\Delta T_x \mid T_{Ww}$) and T_W on the TX_x day ($\Delta T_W \mid TX_x$) will increase by 3 °C–6 °C and 2 °C–4 °C, respectively, as both heat and humidity intensify for the most extreme temperatures (figures 2(a), (b)). Because T_x influences T_W, changes in both variables interact across their distributions. For example, T_x and T_W are negatively amplified on the T_{Ww} and TX_x days, respectively, robustly showing less to no warming (−1 °C to −0.5 °C) as compared with their respective seasonal 50th percentile changes in parts of the subtropics and mid-latitudes (figures 2(c), (d)). This means that on the future days that have the year's hottest temperatures, the increase in humid-heat intensity is projected to be less than the median increase across the warm season. Thus the nonlinear increase in T_x does not to appear drive a nonlinear increase in T_W. Globally, this interactive negative amplification occurs across the top quartile of both the T_x and T_W distributions (figures 2(e), (f)).

Our above analysis highlights that conditions associated with T_x amplification dampen increases in T_W on days at high T_x percentiles (figures 2(d), (f)), while conditions associated with T_W amplification dampen increases in T_x on days at high T_W percentiles (figures 2(c), (e)). These results suggest that nonlinear increases in extreme temperatures alone are insufficient to cause nonlinear increases in humid-heat extremes. We explore this result by demonstrating how interactions between T_x and T_W are mediated by changes in the evaporative fraction (EF), defined as the ratio of the latent heat flux to the total heat flux, and specific humidity. Prior work has linked T_x amplification to land surface drying and associated declines in EF [23]. We confirm this result, showing that EF has a more negative change (drying) on days above the 50th T_x percentile, and a more positive change on days below it (figures 3(a); S2(a)). In addition, relative EF change across the T_W distribution is generally more positive on days above the 50th T_W percentile (figures 3(b); S2(b)). Together, these results suggest

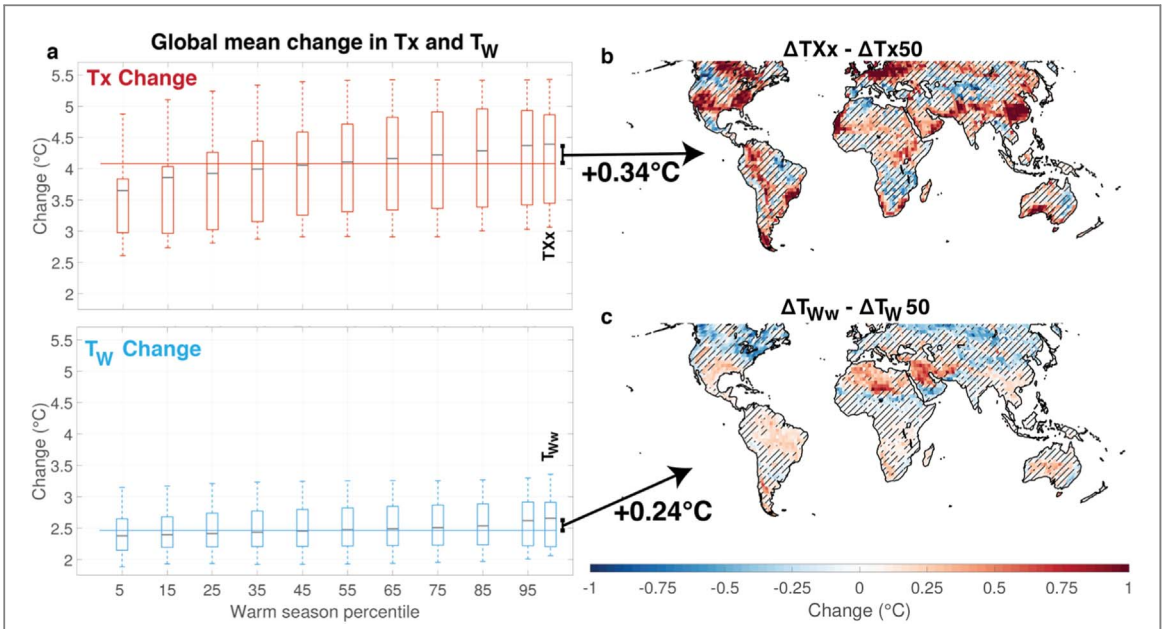

Figure 1. Amplified changes in T_x and T_W. (a) Projected changes in 2061–2085 versus 1981–2005 under RCP 8.5 for globally averaged daily maximum temperature (red; T_x) and estimated daily maximum wet bulb temperature (blue; T_W) across each variable's distribution. Boxplots show the 10th–90th percentile range across the multi-model ensemble. Horizontal red and blue lines show the multi-model median warm season 50th percentile change in T_x and T_W, respectively. (b) T_x amplification on the TX_x day ($\Delta TX_x - \Delta T_x50$), defined as the multi-model median projected change in TX_x minus the projected change in the warm season 50th percentile T_x. Globally averaged T_x amplification is 0.34 °C. (c) T_W amplification on the T_{Ww} day ($\Delta T_{Ww} - \Delta T_W50$), defined as the multi-model median change in T_W on the T_{Ww} day minus the projected change in the warm season 50th percentile T_W. Globally averaged T_W amplification is 0.24 °C. Hatching in (b) and (c) indicates less than 2/3 model agreement on the sign of the amplification.

that the highest T_x days will become relatively drier while the highest T_W days will become relatively wetter, and highlight the fact that the hottest days often are not the same as those with the highest T_W values [30].

Specific humidity responds directly to warming due to the ability of warmer air to hold more moisture. At the same time, however, humidity is shaped by the surface drying that is tightly associated with T_x amplification. Concurrent with the relative changes in EF across the T_x and T_W distributions described above are corresponding changes in specific humidity: when EF change is more positive, specific humidity change is also more positive, a direct result of increased moisture available for evaporation. Accordingly, across the T_x distribution, specific humidity change is more negative on days above the 50th T_x percentile and more positive on days below it (figure 3(c)). In contrast, across the T_W distribution, specific humidity change is more positive on days above the 50th T_W percentile and more negative on days below it (figure 3(d)). Thus within the confines of local land-atmosphere coupling, the linkages between T_x amplification and T_W change center around land surface drying, as indicated by declines in EF. As the surface dries, EF declines, energy is preferentially partitioned to sensible rather than latent heat flux, and temperatures rise more. At the same time, the lack of surface moisture for evaporation dampens the increase in specific humidity, creating a drier but hotter environment on days in the top half of the T_x distribution. The opposite effect occurs on days in the top half of the T_W distribution.

Figure 4 shows the total effect of T_x amplification on T_W change on days above the 50th T_x percentile relative to T_W change at the 50th T_x percentile, encompassing the combined effects of temperature and humidity. There is model agreement on the negative amplification of T_W change associated with T_x amplification in North America, Europe, and Central Asia, regions where the specific humidity component of T_x amplification is projected to strongly dampen T_W (figure S5(b)), and its temperature component is projected to have weak effects on T_W (figure S5(a)). Here, T_W increases are projected to be less than they would be in a world with only linear temperature and specific humidity changes. In much of the rest of the world, there is not model agreement on the direction of T_W change associated with T_x amplification. In these regions, the generally positive effect of the temperature component and the negative effect of the specific humidity component on T_W balance out, making the magnitude of T_W amplification small and its sign uncertain. However, the individual effects of the temperature and specific humidity components of T_x amplification on T_W change are large, meaning that small differences in either component could strongly affect T_W change (figure S5).

Because T_x amplification can contribute to the magnitude of T_W increases in some regions, we seek to clarify the implications of T_x amplification-induced T_W changes on people. We do this by examining how

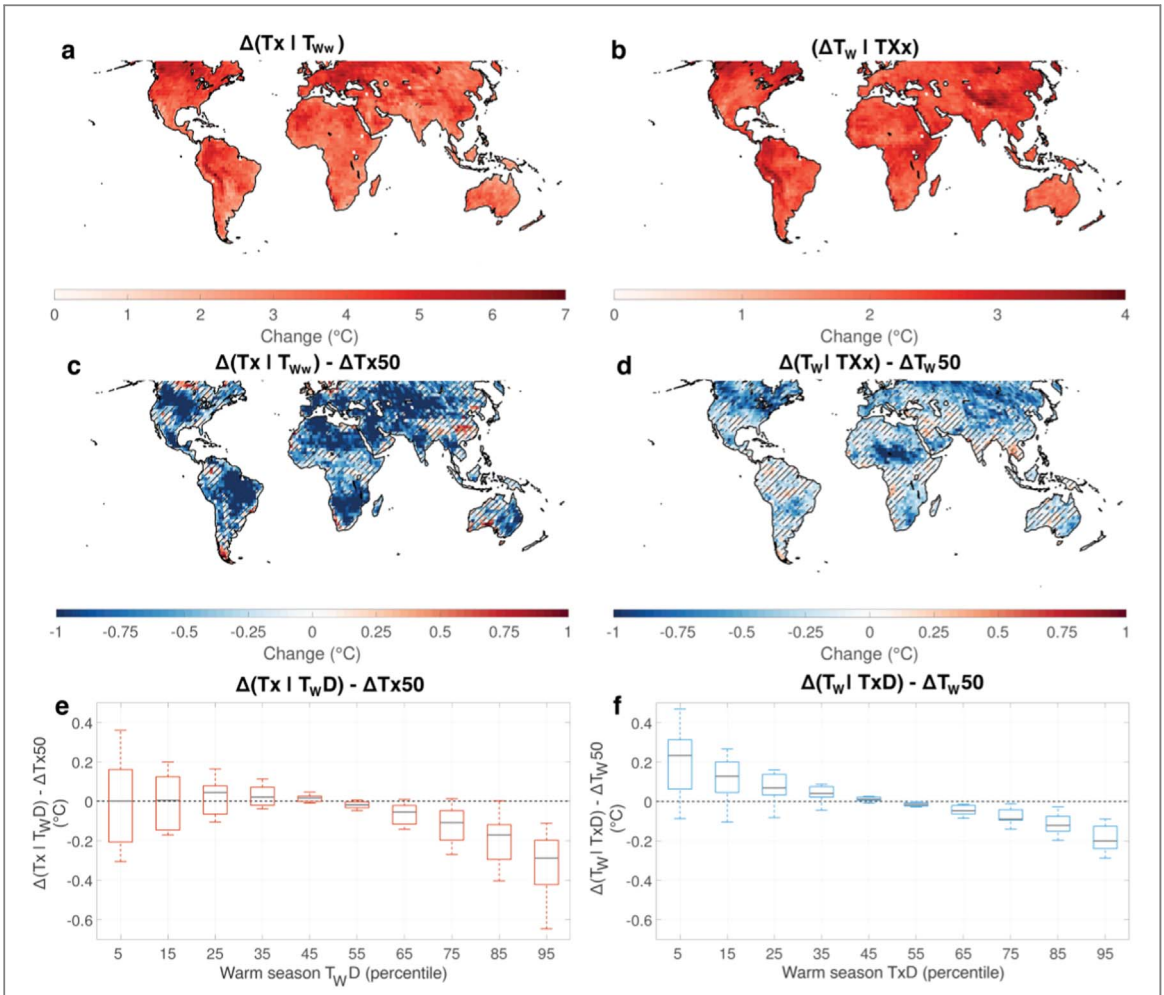

Figure 2. Interactions between T_x and T_W change. (a) Multi-model median projected change in T_x on the T_{Ww} day ($\Delta(T_x \mid T_{Ww})$). (b) Multi-model median projected change in T_W on the TX_x day ($\Delta(T_W \mid TX_x)$). (c) T_x amplification on the T_{Ww} day, defined as the multi-model median projected change in T_x on the T_{Ww} day minus the projected change in warm season 50th percentile T_x ($\Delta(T_x \mid T_{Ww}) - \Delta T_x50$). (d) T_W amplification on the TX_x day, defined as the multi-model median projected change in T_W on the TX_x day minus the projected change in warm season 50th percentile T_W ($\Delta(T_W \mid TX_x) - \Delta T_W50$). Hatching in (c) and (d) indicates less than 2/3 model agreement on the sign of the amplification. (e) Multi-model median global mean T_x amplification across the T_W distribution ($\Delta(T_x \mid T_WD) - \Delta T_x50$). (f) Multi-model median global mean T_W amplification across the T_x distribution. Boxplots show the 10th–90th percentile range across the model ensemble.

T_x amplification contributes to changes in the frequency of T_W days above critical wet bulb thresholds. T_W proxies the effectiveness of evaporative cooling for people, and global mean climate warming will increase the frequency of extreme humid-heat events everywhere. The number of days with a T_W above 27 °C, a level above which mortality is observed to rise in cities across the United States (figure S6), is projected to increase by 5–50 or more days per year in much of the tropics and mid-latitudes, irrespective of T_x amplification (figure 5(a)). Such a response causes increases in global population exposure to T_W thresholds from 27 °C to 31 °C of 25 to 150 billion person days per year, respectively (figure 5(b)) under a scenario of population growth consistent with RCP 8.5 (see Data and methods).

The T_W change due to T_x amplification generally reduces the occurrence of extreme humid-heat events above a T_W of 27 °C in eastern North America and Europe (−2 to −4 d per year) and has little effect on their occurrence in the tropics (figure 5(c)). These reductions in occurrence as compared to a world with linear temperature and specific humidity change make a substantial contribution (−10 to −50%; figure S7) to the overall changes in the frequency of humid-heat extremes in Europe and eastern North America shown in figure 5(a). Because most of the highest T_W values occur in the tropics where T_x amplification has uncertain and near zero effect on T_W change, the globally-averaged effect of T_x amplification is to slightly reduce the number of extreme T_W days exceeding thresholds ranging from 27 °C to 31 °C by 0.1 to 1 day per year, respectively (figure 5(d)). Additionally, because many of the regions where the effect of T_x amplification on T_W change is uncertain are also densely populated, T_x amplification is projected to result in −3 to +2.5 billion more annual person-days per year of exposure to T_W values above 27 °C.

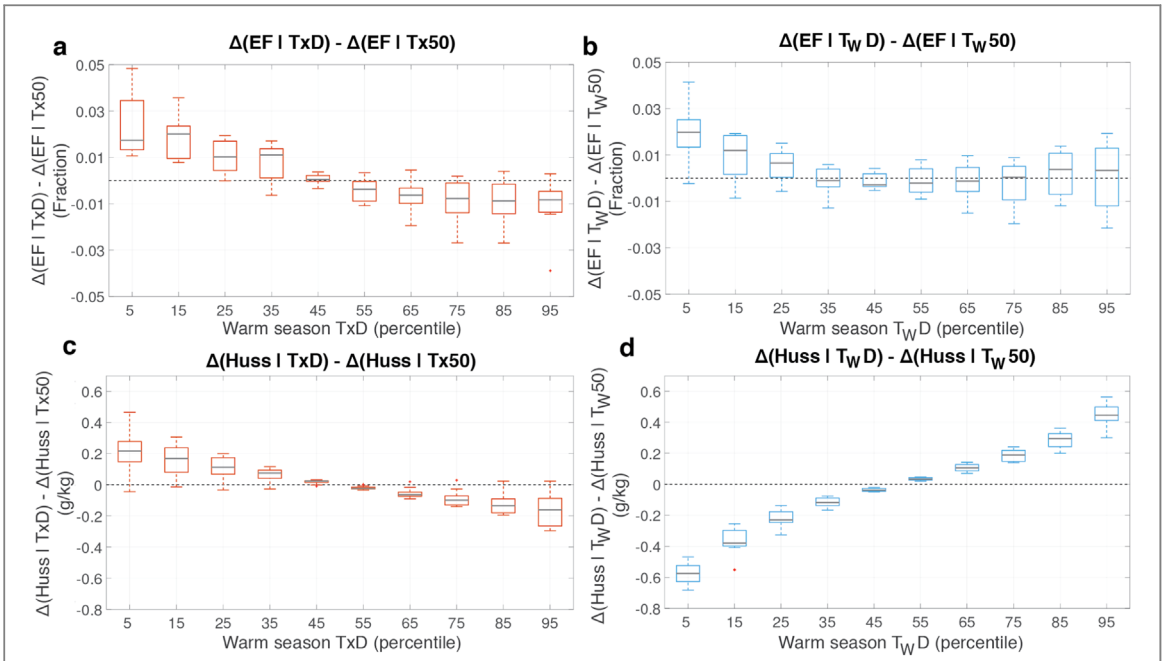

Figure 3. Evaporative fraction and specific humidity changes across the T_x and T_W distributions. (a) EF amplification, defined as the change in EF on days in each T_x decile, relative to the change at the 50th percentile (denoted as $\Delta(\mathrm{EF} \mid T_xD) - \Delta(\mathrm{EF} \mid T_x50)$). (b) EF amplification, defined as the change in EF on days in each T_W decile, relative to the change at the 50th percentile (denoted as $\Delta(\mathrm{EF} \mid T_WD) - \Delta(\mathrm{EF} \mid T_W50)$). (c) Specific humidity amplification, defined as the change in specific humidity on days in each T_x decile, relative to the change at the 50th percentile (denoted as $\Delta(\mathrm{Huss} \mid T_xD) - \Delta(\mathrm{Huss} \mid T_x50)$). (d) Specific humidity amplification, defined as the change in specific humidity on days in each T_W decile, relative to the change at the 50th percentile (denoted as $\Delta(\mathrm{Huss} \mid T_WD) - \Delta(\mathrm{huss} \mid T_W50)$). Boxplots show the 10th–90th percentile range across models.

Discussion and conclusions

Our results show that in the global mean, nonlinear T_x increases are counterbalanced by the dampened increases in specific humidity associated with T_x amplification, resulting in near-linear changes in the T_W distribution (figures 1(a), 3(c), (d)). This global-scale linearity, however, belies important variations in T_x-amplified T_W changes at the regional scale: T_x amplification generally dampens the warm season mean T_W increase in mid-latitudes where warm season moisture is limited (figure 4), and has little or uncertain effect on T_W change in the tropics. This response of T_W is tightly coupled to the specific humidity change that is projected on hot days (figure 3(c)). Globally averaged, T_x amplification serves to slightly reduce the frequency of extreme T_W values of 27 °C or higher as compared to a world with only linear temperature and specific humidity change, a result dominated by eastern North America and Europe where robust warm season mean drying is projected. Because models suggest that declines in surface moisture (proxied by the evaporative fraction) are associated with amplified warming of the hottest temperatures, our results show that more warming of hot extremes can paradoxically reduce the occurrence of humid-heat extremes in some mid-latitude regions.

Land-atmosphere feedbacks play a role in controlling temperature extremes [23, 40], and our results demonstrate that such feedbacks also exert an important influence over the change in T_W extremes. On extreme T_W days, specific humidity is the primary driver of T_W change, while temperature is the primary driver of T_W change on extreme T_x days (figure S8). Accordingly, within the context of land-atmosphere feedbacks, the extent to which T_x amplification modifies extreme T_W change largely depends on how strongly specific humidity responds to surface drying. At the same time, we note that recent work [41] has detailed the importance of atmospheric dynamics and moisture advection in controlling continental humidity; such processes will also influence the changes in humid-heat.

These results emphasize the need for more research investigating the interactions among precipitation, soil moisture, vegetation, and surface heat fluxes, along with their representations in climate models [22]. In particular, the most extreme T_W events often occur along coastlines, making the model parameterizations of sub-grid scale and coastal processes of particular interest. Future increases in model resolution may enable study of these coastal regions with strong temperature and humidity gradients. In this work, we focus on the thermodynamic drivers of nonlinear temperature and T_W change. However, changes in atmospheric circulation patterns have been shown to influence the occurrence frequency of extreme temperature events in the historical record [42], and it is likely that dynamical changes may influence T_W extremes as well.

We have estimated this relationship between T_x amplification and its associated specific humidity

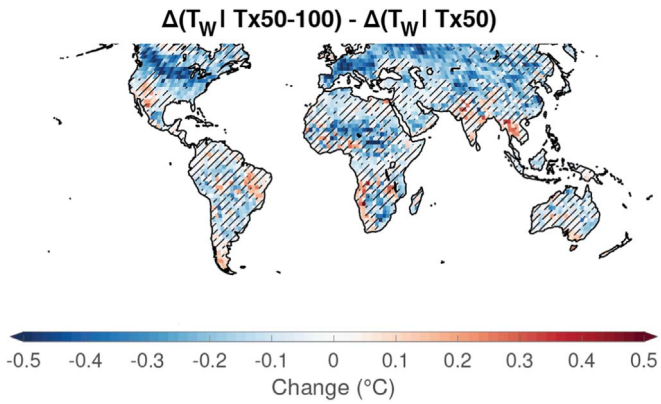

Figure 4. The effect of amplified T_x and specific humidity change on T_W amplification. Multi-model median estimated warm season T_W amplification from T_x amplification ($\Delta(T_W \mid T_x50–100) - \Delta(T_W \mid T_x50)$). This amplification is defined as the change in T_W across the top half of the T_x distribution (T_x50–100) minus the T_W change that occurs at the 50th percentile of the T_x distribution (see Methods). Hatching indicates less than 2/3 model agreement on the sign of the change.

change in 16 global climate models and four climate regions, but the extent to which T_x changes vary within and across simulations may have a substantial effect on T_W change. There is evidence that models may misrepresent the strength of land-atmosphere coupling in some contexts [32], and thus also misrepresent the relationships among evaporative fraction, temperature, and specific humidity that drive T_x amplification. Further, because of the dynamical processes that determine moisture advection from the ocean to the land, uncertainty in both ensemble and model representations of internal variability and surface processes will shape uncertainty in how humid such heat extremes become. Because T_x amplification generally has a negative influence on T_W, an overestimation of the strength of this amplification could result in real-world T_W values increasing more than projected.

Such structural and dynamical uncertainties, however, are crucial to preserve in the diagnosis of the risks posed by humid-heat events. While the magnitude of projected extreme T_W increases across the CMIP5 model ensemble are smaller than for T_x due to the countervailing effects of temperature and humidity change [43], human physiology and health is far more sensitive to small changes in the tails of T_W than in temperature alone. This suggests that small uncertainties in T_W projections can translate into large uncertainties in the risks of health impacts from humid-heat extremes. Accordingly, it is important that impacts-focused research recognize and present the wide range of projected extreme heat and humid-heat outcomes to best position effective climate risk management [44]. It is equally important to consider the spatial heterogeneity of extreme humid-heat and human mortality across the world. In the United States, where air conditioning is widely accessible and most people do not work outdoors, daily mortality begins to sharply increase above T_W values of approximately 27 °C (figure S6). While there may be variation in the mortality response to humid-heat in regions in the tropics and subtropics that regularly experience heat stress, human tolerance to high T_W values is constrained by physiology [1, 29]. Additionally, in regions where baseline health is lower, air conditioning is more expensive or unavailable, and a higher fraction of people perform outdoor physical labor, mortality could respond more sharply to humid-heat than in the US. A more detailed understanding of the regional variation in mortality responses to humid-heat is constrained by health data availability. Given the potential for T_W values to approach the theoretical limits of human tolerance (35 °C), more research is urgently needed to bound the health risks posed by frequent, unprecedented humid-heat in densely populated parts of the world.

Acknowledgments

We acknowledge the World Climate Research Programme's Working Group on Coupled Modelling, which is responsible for CMIP, and we thank the climate modeling groups for producing and making available their model output. For CMIP the US Department of Energy's Program for Climate Model Diagnosis and Intercomparison provides coordinating support and led development of software infrastructure in partnership with the Global Organization for Earth System Science Portals.

Funding

Funding for this work was provided by the Dartmouth Neukom Institute and NSF Award OIA 1556770.

Author contributions

E D C, J S M, R M H, and J M W conceived of the study. E D C and J S M designed the analysis. E D C performed the analysis. E D C, J S M, R M H, and J M

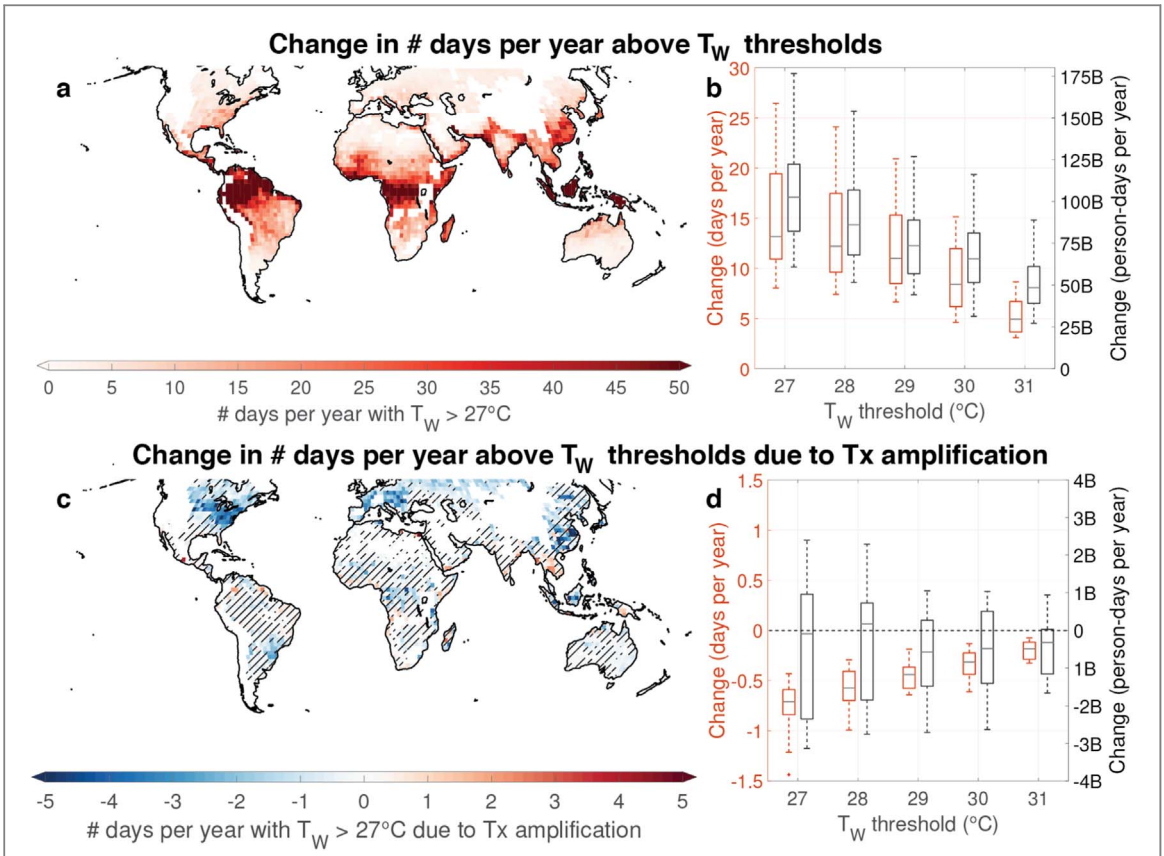

Figure 5. The influence of T_x amplification on the frequency of extreme humid-heat events. (a), (c) Multi-model median additional number of days per year with a T_W exceeding 27 °C due to the (a) all T_W warming under RCP 8.5 and (c) the estimated T_x amplification-driven T_W change (the result shown in figure 4). Hatching indicates less than 2/3 model agreement on the direction of change. (b), (d) Globally averaged additional number of days per year exceeding T_W thresholds from 27 °C–31 °C due to (b) all T_W warming under RCP 8.5 and (d) the estimated T_x amplification-driven T_W change (red), and the projected change in the number of person-days per year of population exposure to these T_W thresholds (black). Boxplots show the 10th–90th percentile range across the model ensemble.

W interpreted the results. E D C and J S M wrote the manuscript with contributions from R M H and J M W.

Competing interests

The authors have no competing interests.

Data and materials availability

Raw CMIP5 data is freely available from the Earth System Research Grid. Intermediate data and processing software is available at www.ethancoffel.com/data/nonlinearT.

ORCID iDs

Ethan D Coffel https://orcid.org/0000-0003-3172-467X
Radley M Horton https://orcid.org/0000-0002-5574-9962
Jonathan M Winter https://orcid.org/0000-0003-1261-4774
Justin S Mankin https://orcid.org/0000-0003-2520-4555

References

[1] Coffel E D *et al* 2018 The science of adaptation to extreme heat *Resilience—The Science of Adaptation to Climate Change* ed T Frank and Z Zommers (Amsterdam: Elsevier)
[2] Glaser J *et al* 2016 Climate change and the emergent epidemic of CKD from heat stress in rural communities: the case for heat stress nephropathy *Clin. J. Am. Soc. Nephrol.* **11** 1472–83
[3] Moore F C and Diaz D B 2015 Temperature impacts on economic growth warrant stringent mitigation policy *Nat. Clim. Change* **5** 127–31
[4] Burke M, Hsiang S M and Miguel E 2015 Global nonlinear effect of temperature on economic production *Nature* **527** 235–9
[5] Lesk C, Coffel E, D'Amato A W, Dodds K and Horton R 2017 Threats to North American forests from southern pine beetle with warming winters *Nat. Clim. Change* **7** 713-7
[6] Lesk C, Rowhani P and Ramankutty N 2016 Influence of extreme weather disasters on global crop production *Nature* **529** 84–7
[7] Schlenker W and Roberts M J 2009 Nonlinear temperature effects indicate severe damages to U.S. crop yields under climate change *Proc. Natl Acad. Sci.* **106** 15594–8
[8] Coffel E D, Thompson T R and Horton R M 2017 The impacts of rising temperatures on aircraft takeoff performance *Clim. Change* **144** 381-8

[9] Coffel E and Horton R 2015 Climate change and the impact of extreme temperatures on aviation *Weather. Clim. Soc.* **7** 94–102
[10] Auffhammer M, Baylis P and Hausman C H 2017 Climate change is projected to have severe impacts on the frequency and intensity of peak electricity demand across the United States *Proc. Natl Acad. Sci. USA* **114** 1886–91
[11] Horton R M, Mankin J S, Lesk C, Coffel E and Raymond C 2016 A review of recent advances in research on extreme heat events *Curr. Clim. Change Rep.* **2** 242–59
[12] Horton R M, Coffel E D, Winter J M and Bader D A 2015 Projected changes in extreme temperature events based on the NARCCAP model suite *Geophys. Res. Lett.* **42** 7722-31
[13] Rahmstorf S and Coumou D 2012 Increase of extreme events in a warming world *Proc. Natl Acad. Sci.* **109** 4708–4708
[14] Meehl G A and Tebaldi C 2004 More intense, more frequent, and longer lasting heat waves in the 21st century *Science* **305** 994–7
[15] Miralles D G, Teuling A J, van Heerwaarden C C and Vilà-Guerau de Arellano J 2014 Mega-heatwave temperatures due to combined soil desiccation and atmospheric heat accumulation *Nat. Geosci.* **7** 345–9
[16] Hirschi M *et al* 2011 Observational evidence for soil-moisture impact on hot extremes in southeastern Europe *Nat. Geosci.* **4** 17–21
[17] Zampieri M *et al* 2009 Hot European summers and the role of soil moisture in the propagation of mediterranean drought *J. Clim.* **22** 4747–58
[18] Seneviratne S I *et al* 2010 Investigating soil moisture-climate interactions in a changing climate: a review *Earth-Sci. Rev.* **99** 125–61
[19] Skinner C B, Poulsen C J and Mankin J S 2018 Amplification of heat extremes by plant CO2 physiological forcing *Nat. Commun.* **9** 1–11
[20] Mueller N D *et al* 2016 Cooling of US Midwest summer temperature extremes from cropland intensification *Nat. Clim. Change* **6** 317–22
[21] Mankin J S, Smerdon J E, Cook B I, Williams A P and Seager R :10.1175/JCLI-D-17-0213.1 2017 The curious case of projected 21st-century drying but greening in the American West *J. Clim.* **30** 869-710
[22] Mankin J S *et al* 2018 Blue water trade-offs with vegetation in a CO2-enriched climate *Geophys. Res. Lett.* **45** 3115–25
[23] Donat M G, Pitman A J and Seneviratne S I 2017 Regional warming of hot extremes accelerated by surface energy fluxes *Geophys. Res. Lett.* **44** 7011–9
[24] Coffel E D, Horton R M and De Sherbinin A 2018 Temperature and humidity based projections of a rapid rise in global heat stress exposure during the 21st century *Environ. Res. Lett.* **13** 014001
[25] Pal J S and Eltahir E A B 2015 Future temperature in southwest Asia projected to exceed a threshold for human adaptability *Nat. Clim. Change* **18203** 1–4
[26] Im E-S, Pal J S and Eltahir E A B 2017 Deadly heat waves projected in the densely populated agricultural regions of South Asia *Sci. Adv.* **3** 1–8
[27] Kang S and Eltahir E A B 2018 North China plain threatened by deadly heatwaves due to climate change and irrigation *Nat. Commun.* **9** 2894
[28] Willett K M and Sherwood S 2012 Exceedance of heat index thresholds for 15 regions under a warming climate using the wet-bulb globe temperature *Int. J. Climatol.* **32** 161–77
[29] Sherwood S C and Huber M 2010 An adaptability limit to climate change due to heat stress *Proc. Natl Acad. Sci.* **107** 9552–5
[30] Raymond C, Singh D and Horton R M 2017 Spatiotemporal patterns and synoptics of extreme wet-bulb temperature in the contiguous United States *J. Geophys. Res. Atmos.* **122** 13108-24
[31] Seneviratne S I, Lüthi D, Litschi M and Schär C 2006 Land–atmosphere coupling and climate change in Europe *Nature* **443** 205–9
[32] Ukkola A M, Pitman A J, Donat M G, De Kauwe M G and Angélil O 2018 Evaluating the contribution of land-atmosphere coupling to heat extremes in CMIP5 models *Geophys. Res. Lett.* **45** 9003–12
[33] Taylor K E, Stouffer R J and Meehl G A 2012 An overview of CMIP5 and the experiment design *Bull. Am. Meteorol. Soc.* **93** 485–98
[34] Moss R H *et al* 2010 The next generation of scenarios for climate change research and assessment *Nature* **463** 747–56
[35] Davies-Jones R 2008 An efficient and accurate method for computing the wet-bulb temperature along pseudoadiabats *Mon. Weather Rev.* **136** 2764–85
[36] Buzan J R, Oleson K and Huber M 2015 Implementation and comparison of a suite of heat stress metrics within the community land model version 4.5 *Geosci. Model Dev.* **8** 151–70
[37] Kopp R E Wet bulb calculation (http://www.bobkopp.net/software/)
[38] O'Neill B C *et al* 2014 A new scenario framework for climate change research: the concept of shared socioeconomic pathways *Clim. Change* **122** 387–400
[39] Jones B *et al* 2016 Spatially explicit global population scenarios consistent with the Shared Socioeconomic Pathways *Environ. Res. Lett.* **11** 084003
[40] Donat M G, Pitman A J and Angélil O 2018 Understanding and reducing future uncertainty in mid-latitude daily heat extremes via land surface feedback constraints *Geophys. Res. Lett.* (https://doi.org/10.1029/2018GL079128)
[41] Byrne M P and O'Gorman P A 2018 Trends in continental temperature and humidity directly linked to ocean warming *Proc. Natl Acad. Sci.* **115** 4863–8
[42] Horton D E *et al* 2015 Contribution of changes in atmospheric circulation patterns to extreme temperature trends *Nature* **522** 465–9
[43] Fischer E M and Knutti R 2012 Robust projections of combined humidity and temperature extremes *Nat. Clim. Change* **3** 126–30
[44] Kunreuther H *et al* 2013 Risk management and climate change *Nat. Clim. Change* **3** 447–50